

High precision calculations of the $1s^2 2s 2p \ ^1P_1 - 1s^2 2s^2 \ ^1S_0$ spin allowed $E1$ transition in C III

M. Bilal,^{1,2,3} A. V. Volotka,^{1,2} R. Beerwerth,^{1,2,3} J. Rothhardt,^{1,2,4} V. Hilbert,^{1,2,4} and S. Fritzsche^{1,2,3}

¹*Helmholtz-Institut Jena, Fröbelstieg 3, D-07743 Jena, Germany*

²*GSI Helmholtzzentrum für Schwerionenforschung GmbH, Planckstrasse 1, D-64291 Darmstadt, Germany*

³*Theoretisch-Physikalisches Institut, Friedrich-Schiller-Universität Jena, Max-Wien-Platz 1, D-07743 Jena, Germany*

⁴*Fraunhofer Institute for Applied Optics and Precision Engineering, Albert-Einstein-Straße 7, 07745 Jena, Germany*

Large-scale relativistic calculations are performed for the transition energy and line strength of the $1s^2 2s 2p \ ^1P_1 - 1s^2 2s^2 \ ^1S_0$ transition in Be-like carbon. Based on the multiconfiguration Dirac-Hartree-Fock (MCDHF) approach, different correlation models are developed to account for all major electron-electron correlation contributions. These correlation models are tested with various sets of the initial and the final state wave functions. The uncertainty of the predicted line strength due to missing correlation effects is estimated from the differences between the results obtained with those models. The finite nuclear mass effect is accurately calculated taking into account the energy, wave functions as well as operator contributions. As a result, a reliable theoretical benchmark of the $E1$ line strength is provided to support high precision lifetime measurement of the $1s^2 2s 2p \ ^1P_1$ state in Be-like carbon.

I. INTRODUCTION

Our understanding of the structure and dynamics of many-electron atoms and ions depends on a detailed analysis and comparison of theoretical predictions with experimental observations of atomic properties. Two important and complementary properties of atomic states are transition energies and transition rates. For transition energies, the present experimental accuracy reaches the order of $10^{-6} - 10^{-18}$ [1–3]. For this case the interplay between experiment and theory has improved drastically our understanding of different effects, e.g., the Breit interaction, finite nuclear mass, and quantum electrodynamics (QED) effects [4, 5]. This interplay also has great potential in the search for new physics [6].

For transition rates of many-electron atoms and ions, in contrast, most if not all the experiments provide uncertainties in the region of 30%–1%, e.g., see the reviews [7, 8] and references therein. Whereas only a few experiments provide the uncertainty in the region 1%–0.1% with some rare and favorable circumstances mainly for the $M1$ forbidden transitions, e.g., Refs. [9, 10]. In this context, high hopes are pinned on the femtosecond laser technology [11], which has already demonstrated great success in studies of chemical reactions, wave function dynamics, photoionization time delays, etc. The femtosecond laser technology allows to perform the highly accurate pump-probe atomic lifetime measurements. In particular, the so-called pump-probe technique has been used already in the lifetime measurements of the $6P_{3/2}$ excited-state in cesium atom which is relevant to the atomic parity non-conservation [12, 13]. In contrast to neutral atoms, transitions to excited states in ions quickly reach the XUV- or X-ray energy range and, therefore, for the pumping and/or probing processes a high-photon flux of XUV- or X-ray sources is required. For this purpose, for instance, the Linac Coherent Light Source has been employed in the measurement of lifetimes in Ne-like iron

[14]. Recently, it has been also proposed to use a compact high-power XUV-ray source in a combination with the storage ring at GSI to perform precision spectroscopy and lifetime measurements of ions [15]. For this purpose, a novel high-photon flux XUV-radiation source based on the high harmonic generation in argon has been developed, which provides ~ 100 femtosecond pulses at photon energies up to 26.6 eV [16, 17]. As the first experiment, the measurement of the lifetime of the $1s^2 2s 2p \ ^1P_1$ state in Be-like carbon is proposed. The schematic diagram of the proposed experiment is shown in Fig. 1. In principle, the relative accuracy could reach the order $10^{-4} - 10^{-5}$ [15].

The excited state $1s^2 2s 2p \ ^1P_1$ decays to the $1s^2 2s^2 \ ^1S_0$ ground state through a strong spin allowed $E1$ transition. Therefore, the lifetime of the $1s^2 2s 2p \ ^1P_1$ state is defined by the line strength of this strong transition. During past years, various calculations have been reported for this line strength. Among these *ab initio* theories, particularly for the last three decades, are multiconfiguration Hartree-Fock (MCHF) [18], multiconfiguration Dirac-Hartree-Fock (MCDHF) [19–21], many-body perturbation theory (MBPT) [22], configuration-interaction (CI) method based on B-spline basis [23] and configuration-interaction and many-body perturbation theory (CI+MBPT) [24]. As a result, the most accurate theoretical calculations [20, 23] report an accuracy of the order 5×10^{-4} . In view that the expected experimental accuracy is much better, there is a need for further improvements in the theoretical calculations.

Here, we present a detailed calculation of the line strength of the $1s^2 2s 2p \ ^1P_1 - 1s^2 2s^2 \ ^1S_0$ transition in Be-like carbon on account of high precision experiment. We develop various electron correlation models and use orthogonal and nonorthogonal sets of orbitals for the initial and final states in these correlation models. It is found, that the accuracy assessment based on an agreement between the gauges might significantly lead to underestimate the uncertainty. For this reason, we esti-

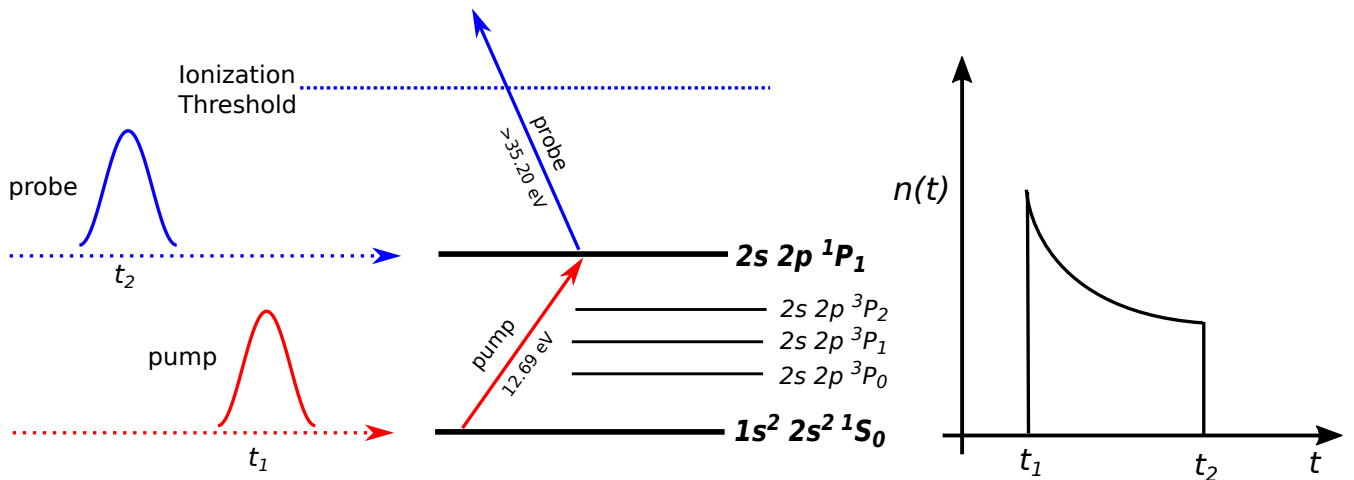


FIG. 1. Scheme of a pump-probe experiment for atomic lifetime measurements of the $1s^2 2s 2p \ ^1P_1$ state in Be-like carbon. At time t_1 the XUV-pump pulse excites the $1s^2 2s^2 \ ^1S_0$ ground state of the Be-like carbon sample to the $1s^2 2s 2p \ ^1P_1$ excited state. The population $n(t)$ of the excited state $\ ^1P_1$ decays then exponentially. A second and temporally delayed XUV-probe pulse probes the rest population of the excited state at time t_2 by ionizing Be-like carbon ion and maps out the exponential curve from which the decay rate is determined.

mate the uncertainty from the differences between the results obtained within all the correlation models developed. In addition, the finite nuclear mass effect on the line strength is evaluated and its gauge invariance is demonstrated after taking into account the recoil correction to the transition operator. As a result, the calculated line strength amounts to 2.43926(37) with the relative accuracy 1.5×10^{-4} .

The following parts of the paper are structured as follows. In Sec. II, we present the underlying theory for the calculation of the transition energy and line strength. Details of the correlation models and results obtained are explained in Sec. III. In Sec. IV, we present theoretical methods for the finite nuclear mass effect. In the final section, we compare the obtained results with other theories and experiments and present the conclusion.

The atomic units ($\hbar = 1$, $e = 1$, $m_e = 1$) are used throughout the paper unless stated otherwise.

II. THEORETICAL METHODS

To effectively evaluate the electron-electron correlation effects, we apply systematically enlarged many-electron wave functions by using the general purpose relativistic atomic structure package GRASP2K [25]. This package implements the multiconfiguration Dirac-Hartree-Fock (MCDHF) method in jj -coupling [26, 27]. In this method, the wave function Ψ of a state labelled Γ , total angular momentum quantum number J and parity π is referred to as an atomic state function (ASF) which is represented as $\Psi(\Gamma; \pi J)$. It is an approximate eigenfunc-

tion of the Dirac-Coulomb Hamiltonian given by

$$\hat{H}_{\text{DC}} = \sum_{i=1}^N \left[c\boldsymbol{\alpha}_i \cdot \mathbf{p}_i + (\beta_i - 1)c^2 - V(r_i) \right] + \sum_{i<j}^N \frac{1}{r_{ij}}, \quad (1)$$

where c is the speed of light, $\boldsymbol{\alpha}$ and β are (4×4) Dirac matrices, $V(r_i)$ is the potential of a two parameter Fermi nuclear charge distribution and r_{ij} is the distance between electrons i and j .

The ASF $\Psi(\Gamma; \pi J)$ is expanded in the basis of configuration state functions (CSFs) of the same symmetry:

$$\Psi(\Gamma; \pi J) = \sum_{j=1}^{n_c} c_j \Phi(\gamma_j; \pi J), \quad (2)$$

where n_c is the number of CSFs, c_j are the mixing coefficients and γ_j denotes the orbital occupancy and angular coupling scheme of the j -th CSF. The CSFs $\Phi(\gamma_j; \pi J)$ are a linear combination of Slater determinants of one electron Dirac orbitals,

$$\phi_{n\kappa,m}(\mathbf{r}) = \frac{1}{r} \begin{pmatrix} P_{n\kappa}(r) \chi_{\kappa}^m(\theta, \varphi) \\ iQ_{n\kappa}(r) \chi_{-\kappa}^m(\theta, \varphi) \end{pmatrix}. \quad (3)$$

Here, κ is the relativistic angular momentum quantum number, $P_{n\kappa}(r)$ and $Q_{n\kappa}(r)$ are the large and small radial components of the one electron wave functions represented on a logarithmic grid, and χ_{κ}^m is the spinor spherical harmonic. The radial part of the Dirac orbitals and the expansion coefficients c_j are optimized to self consistency from a set of equations which result from applying the variational principle in Dirac-Coulomb approximation [28]. Here we have a choice of simultaneous or separate optimization of the orbitals for the desired ASFs. In the optimal level (OL) scheme a variational functional

is constructed to minimize the energy for only one ASF, whereas in the extended optimal level (EOL) scheme the calculations can be extended to include several ASFs. In the latter case, the energy functional contains weights for the levels under consideration.

The line strength of the transition is defined as a square of the reduced nondiagonal matrix element of the electromagnetic operator:

$$S = |\langle \Psi(\Gamma; \pi J) || \mathbf{T} || \Psi(\Gamma'; \pi' J') \rangle|^2, \quad (4)$$

which after the optimization of the wave functions for the states $\Psi(\Gamma; \pi J)$ and $\Psi(\Gamma'; \pi' J')$ is calculated as

$$S = \left| \sum_{j,k} c_j c'_k \langle \Phi(\gamma; \pi J) || \mathbf{T} || \Phi(\gamma'; \pi' J') \rangle \right|^2. \quad (5)$$

Here, \mathbf{T} is $E1$ transition operator [26]

$$\begin{aligned} T_M^l = & \frac{\sqrt{2\pi c}}{\omega} \sum_i^N \left[-\sqrt{6} j_1(\omega r_i/c) Y_{1M}(\mathbf{n}_i) \right. \\ & \left. + 3j_2(\omega r_i/c) c\alpha_i \cdot \mathbf{Y}_{1M}^2(\mathbf{n}_i) \right] \end{aligned} \quad (6)$$

in the length gauge and

$$\begin{aligned} T_M^v = & \frac{\sqrt{2\pi c}}{\omega} \sum_i^N \left[-\sqrt{2} j_0(\omega r_i/c) c\alpha_i \cdot \mathbf{Y}_{1M}^0(\mathbf{n}_i) \right. \\ & \left. + j_2(\omega r_i/c) c\alpha_i \cdot \mathbf{Y}_{1M}^2(\mathbf{n}_i) \right] \end{aligned} \quad (7)$$

in the velocity gauge. Here, ω is the transition energy, Y_{JM} are the spherical harmonics, \mathbf{Y}_{JM}^L are the spherical vectors, and $j_J(\omega r/c)$ is the spherical Bessel function. The operators (6) and (7) are used for the present calculations of the line strengths in length and velocity gauges. However, in order to investigate the dependence of the line strength on the transition energy we expand the Bessel functions $j_J(\omega r/c) \approx (\omega r/c)^J / (2J+1)!!$, the so-called long-wavelength approximation $\omega/c \ll 1$, and retain only the leading term in the power series expansion. In such a way the line strength takes a form:

$$S^l \approx \left| \left\langle \Psi(\Gamma; \pi J) \left\| \sum_i^N \mathbf{r}_i \right\| \Psi(\Gamma'; \pi' J') \right\rangle \right|^2 \quad (8)$$

in the length gauge and

$$S^v \approx \frac{c^4}{\omega^2} \left| \left\langle \Psi(\Gamma; \pi J) \left\| \sum_i^N \alpha_i \right\| \Psi(\Gamma'; \pi' J') \right\rangle \right|^2 \quad (9)$$

in the velocity gauge. From the expressions (8) and (9) one can see, that the leading term of the line strength in the length form is insensitive to the transition energy whereas in the velocity form it is proportional to ω^{-2} . Based on these observations one can introduce the semi-empirical correction to the line strength in the velocity gauge by adjusting the transition energy to a more accurate, e.g., experimental, value, i.e., $\Delta S^v =$

$(\omega^2 - \omega_{\text{exp}}^2) / \omega_{\text{exp}}^2 S^v$. Such a correction allows to take partially into account the missing correlation contributions. The line strength in the velocity gauge adjusted in this way $S_{(\text{exp})}^v$ is typically much closer to the value in the length gauge S^l . Generally, the gauge invariance should be restored when all correlation effects are taken into account, both for the transition matrix element and transition energy, which was explicitly demonstrated in the framework of the relativistic many-body perturbation theory [29] and QED formalism [30]. In view of this, the excellent agreement between the gauges after adjustment suggests that the remaining unaccounted correlation effects to the transition amplitude are rather small. As a result, the difference between the line strengths calculated in the length gauge and adjusted value in the velocity gauge is employed for the theoretical error estimation [31, 32]. However, it is still possible that the remaining unaccounted correlation effects not only reduce the discrepancy between the gauges but also shift both values by an amount, which is much larger than the difference between the gauges after adjustment.

III. CORRELATION MODELS

In a view of an absence of strong criteria for the uncertainty estimation of the calculated line strength, we performed the MCDHF calculations for different correlations models. Among those models, we choose only four models based on the accuracy criterion for the transition energy as it is compared with the experimental energy. These four models were based on separate and simultaneous (orthogonal and nonorthogonal) set of orbitals for the ground and excited states. In each model, the correlations were incorporated by systematically extending the calculations in a series of steps. As a first step, the calculations were performed for the lowest order of approximation where the orbitals belonging to so-called reference configurations were spectroscopically optimized, i.e., orbitals were required to have a node structure similar to the corresponding hydrogenic orbitals [27]. Here the reference configurations for the first three models were $\{1s^2 2s^2, 1s^2 2p^2\}$ for the 1S_0 ground state and $\{1s^2 2s 2p\}$ for the 1P_1 excited state. For the fourth model, the reference configurations were increased and we explain its details later in this section. In the latter steps, the calculations were extended by expanding the basis set of CSFs using the active set approach. In this approach, the correlations are incorporated by virtually exciting the electrons from spectroscopic reference configurations to a set of orbitals called the active set of orbitals. We increased the active set by adding a layer of correlation orbitals but optimized only the outermost layer and kept the remaining orbitals fixed from the previous step of calculations.

We now explain how valence-valence (VV), core-valence (CV) and core-core (CC) correlations were incorporated. We started to expand the basis set by adding the CSFs that are generated from the configurations

$1s^2nl^n'l'$ which result from single and double (SD) excitations from outer shells of the reference configuration. These CSFs account VV correlations and the calculations are named as VV calculations. To each layer of VV correlation calculations, we then added CSFs of the configurations $1s2snln'l' + 1s2pnl^n'l'$ which arise from the single excitation from the $1s^2$ core with or without another excitation from the valence shells. These added CSFs account for the CV correlations and the calculations are called VV+CV. Now with each layer of VV+CV correlation calculations, the correlations of two-electron excitations from the $1s^2$ core were included to account for the CC correlations. These additional CSFs arise from the configurations $2s^2nl^n'l' + 2p^2nl^n'l'$ for the 1S_0 state and $2s2pnl^n'l'$ for the 1P_1 state. These correlation cal-

culations are named as VV+CV+CC calculations. In all VV, VV+CV and VV+CV+CC calculations, the active set of orbitals was spanned by the orbitals with principal quantum number $n, n' \leq 15$ and with azimuthal quantum number $l, l' \leq 7$. Finally, the basis set of CSFs was expanded by appending CSFs with configurations arising from single, double, triple and quadruple (SDTQ) excitations from the reference configurations. In the SDTQ excitations the number of CSFs increased very rapidly with the increasing number of orbitals in the active set which challenges the numerical stability and available hardware resources. So the SDTQ excitations were limited only with $n, n' \leq 5$ and $l, l' \leq 4$. These calculation were then extended with SD excitations with remaining layer of correlation orbitals with $n, n' \leq 15$ and $l, l' \leq 7$. We name this final set of calculations as VV+CV+CC:SDTQ.

A. Model 1

In this model the VV and VV+CV calculations were performed by utilizing the OL scheme for the ground and excited state, i.e., for both states orbitals are separately optimized, whereas for the VV+CV+CC as well as VV+CV+CC:SDTQ calculations the spectroscopic orbitals and the correlation orbitals with $n = 3$ were simultaneously optimized using the EOL scheme. Then the calculations after $n = 3$ were extended with a separate set of correlation orbitals (the OL scheme). This model accounts for the correlations in a similar manner as those presented by Jönsson and Froese Fischer [20]. The only difference is that Jönsson and Froese Fischer performed VV+CV+CC:SDTQ calculations with SDTQ excitation until $n = 3$ only and extended their calculations from $n > 3$ with VV+CV type of correlations only.

In Fig. 2 (upper plot) we compare the present calculations of Model 1 with Jönsson and Froese Fischer results [20]. The line strength in length and velocity form is plotted against increasing n of the active set size defining the wave function expansion in respective calculations. It is clearly evident that their two gauges agree perfectly at $n = 8$ once the experimental energy adjustment was applied. Explicitly, the line strength calculated in Ref. [20] amounts to 2.4376 in the length gauge and 2.4366 in the velocity gauge after adjustment, which leads to a tabulated final value 2.4376(13). Despite we can not explicitly reproduce these calculations, our evaluations show the similar effect at $n = 7$ active set layer, where the results obtained in the length and velocity (adjusted) gauges approach each other. However, when the active set size is further extended, one can clearly see that after $n = 7$ layer the results first drift apart and then, again, approach each other but at some different position. These observations lead us to the following conclusions. First, the agreement between gauges might be of an accidental character and, therefore, second, the difference between results in the length and velocity (adjusted) gauges should be very carefully used as a criterion for the error

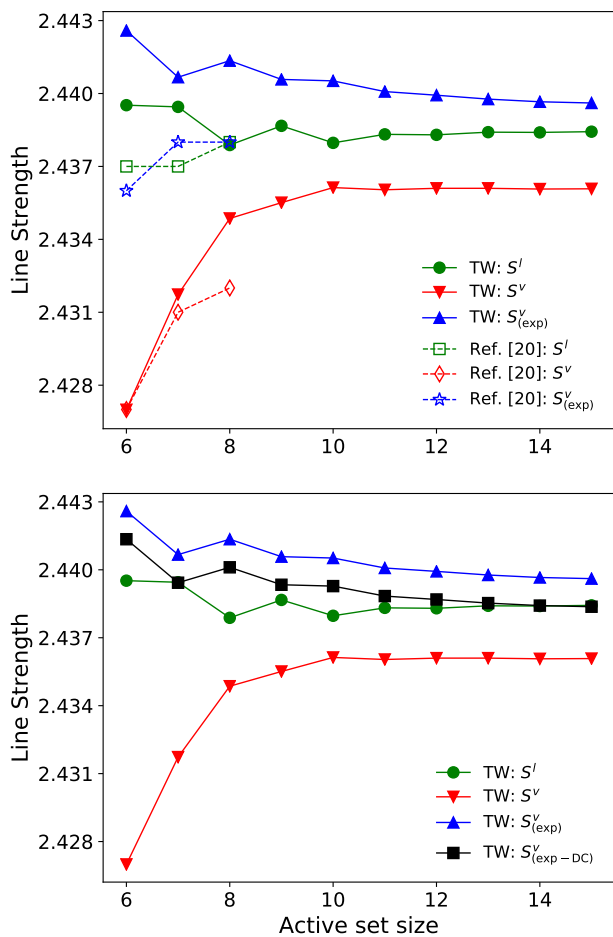


FIG. 2. Comparison of the line strengths evaluated according to the Model 1 (TW) as a function of active set size of the orbitals with the results of Ref. [20]. The green circles, red down triangles, and blue upper triangles display the present calculations in the length gauge S^l as well as in velocity gauges before S^v and after adjustment $S^v_{(\text{exp})}$ to the experimental transition energy ω_{exp} , respectively. The green hollow squares, red hollow diamonds, and blue hollow stars are corresponding values taken from Ref. [20].

TABLE I. Transition energies ω (cm^{-1}) and line strengths S (a.u.) for the $1s^2 2s 2p \ ^1P_1 - 1s^2 2s^2 \ ^1S_0$ transition in Be-like carbon as functions of the active set calculated within Model 1. The line strengths in the length gauge (S^l) are compared with those in the velocity gauge *ab initio* calculated (S^v) and after adjustment to the experimental energy ω_{exp} ($S^v_{(\text{exp})}$) and to the experimental-Dirac-Coulomb energy $\omega_{\text{exp-DC}}$ ($S^v_{(\text{exp-DC})}$). The experimental transition energy is taken from Ref. [33], while the experimental-Dirac-Coulomb energy is evaluated by subtracting the Breit, recoil, and QED corrections from the experimental transition energy.

Active set	ω	S^l	S^v	$S^v_{(\text{exp})}$	$S^v_{(\text{exp-DC})}$
DHF	112 958	2.34092	1.65645	2.01753	2.01651
3s3p3d	104 094	2.51432	2.36757	2.44884	2.44759
4s4p4d4f	103 116	2.45884	2.38001	2.41568	2.41446
5s5p5d5f5g	102 804	2.44978	2.40435	2.42565	2.42442
6s6p6d6f6g6h	102 680	2.43952	2.42699	2.44259	2.44135
7s7p7d7f7g7h7i	102 540	2.43945	2.43173	2.44067	2.43943
8s8p8d8f8g8h8i8k	102 488	2.43788	2.43486	2.44135	2.44011
9s9p9d9f9g9h9i9k	102 459	2.43867	2.43551	2.44058	2.43934
10s10p10d10f10g10h10i10k	102 444	2.43797	2.43613	2.44052	2.43928
11s11p11d11f11g11h11i10k	102 437	2.43832	2.43604	2.44008	2.43884
12s12p12d12f12g12h12i10k	102 432	2.43830	2.43610	2.43993	2.43869
13s13p13d13f13g13h13i10k	102 429	2.43841	2.43610	2.43977	2.43853
14s14p14d14f14g14h14i10k	102 427	2.43840	2.43607	2.43966	2.43842
15s15p15d15f15g15h15i10k	102 426	2.43843	2.43608	2.43961	2.43837
Due to other models	-15				
Breit	-3				
Recoil	-13				
QED	-10				
Total	102 385				
Exp	102 352				
Exp-DC	102 378				

estimation.

Let us mention here another important observation. From the basic theory [29, 30], it is clear that the adjustment should be made to the transition energy which corresponds to the difference of the eigenvalues of the Dirac-Coulomb Hamiltonian in Eq. (1). Therefore, we calculate a so-called experimental-Dirac-Coulomb transition energy $\omega_{\text{exp-DC}}$ as a difference of the experimental value ω_{exp} and the contributions beyond the Dirac-Coulomb approximation, i.e., the Breit interaction, recoil, and QED corrections. The $\omega_{\text{exp-DC}}$ energy is, thus, experimentally deduced fully correlated Dirac-Coulomb transition energy. We compare in Table I as well as in Fig. 2 (lower plot) the line strengths in the length gauge (S^l) and in the velocity gauge (*ab initio*) (S^v) with the adjusted to ω_{exp} ($S^v_{(\text{exp})}$) and to $\omega_{\text{exp-DC}}$ ($S^v_{(\text{exp-DC})}$) values. As one can see from this comparison the values adjusted to the experimental-Dirac-Coulomb energy are much close to the results in the length gauge. In particular, for $n = 15$ layer the relative difference between the gauges amounts to 2×10^{-5} . However, as we mention at the end of Sec. II the agreement between the gauges cannot be uniquely used for the accuracy assessment. For this reason, in the next subsections, we investigate also other correlation models.

B. Model 2

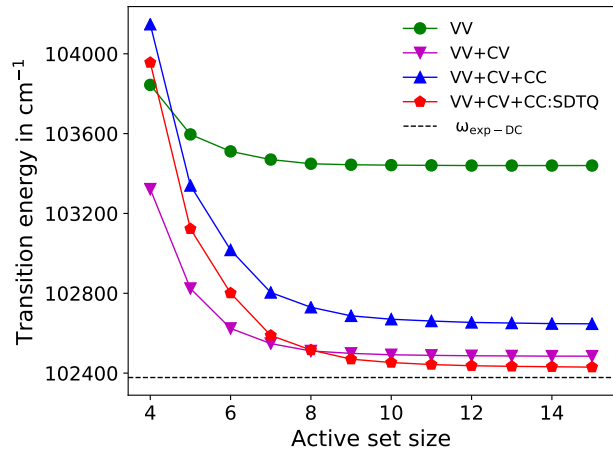


FIG. 3. Extent of different correlations effects to the transition energy with respect to the increasing n of the active set size defining the wave function expansion for the Model 2 calculations. The green circles represent VV correlations, magenta down triangles represent VV+CV, blue upper triangles represent VV+CV+CC, red-pentagons represent VV+CV+CC:SDTQ correlations. Please see the text for the details of different type of the correlations.

Within this model, both the spectroscopic and the

correlations orbitals were separately optimized using the OL scheme for all type of correlations. Hence generated orbitals for both states were not quite orthogonal with each other, which makes the implementation of standard Racah algebra difficult for the calculation of transition amplitude. To deal with this complication, a transformation to a biorthonormal basis was applied together with the counter transformation of the expansion coefficients c_j and c'_k [34].

The calculations within this model show the importance of a common set of orbitals for the core correlations in the framework of MCDHF approach. For the CC effects, it is commonly accepted that these are more balanced if a common orbital basis is used for describing both the states involved in the transition and hence resulting transition energies are more accurate, for details please see the Ref. [35, 36]. This is also obvious from Fig. 3 where the evaluation of different correlations effects to the transition energy is shown with respect to the increasing n of the active set size defining the wave function expansion for the Model 2 calculations. Here the blue upper triangles representing VV+CV+CC correlation results are worse than the magenta down triangles representing VV+CV correlations. However, it is obvious from the red-pentagons representing VV+CV+CC:SDTQ in Fig. 3 that we get the best agreement of the transition energy with the experiment when the TQ excitations are included with SD excitations in the CC correlations. The difference of the final values of the energy of VV+CV+CC:SDTQ calculations with Model 1 and Model 2 is only 0.004%, whereas the length form of the line strength from both models varies only by 0.01%. The fact that TQ contributions are very important is also noticed from the results of Chen, Cheng and Johnson [23] who have also used TQ excitations in building a common set of orbitals in their RCI calculations based on B-spline basis.

C. Model 3

Within this model, both the spectroscopic orbitals and correlations orbitals were simultaneously optimized for the ground and excited states using the EOL scheme for all type of correlations. The so obtained orbitals for both states were orthogonal to each other. As it has been highlighted by Chen, Cheng and Johnson [23] and Savukov [24] that small orbital overlap corrections due to nondiagonal set of orbitals for the initial and final state should not be ignored. Our correlation Model 3 helped to address this issue.

D. Model MR

In this model, the set of spectroscopic reference configurations were expanded to account the missing correlations due to limited SDTQ excitations. We

name it as multi-reference (MR) model. The configurations in MR are expanded in such a way that the CSFs for the MR set had the largest expansion coefficients in the wave functions that were generated by VV+CV+CC:SDTQ calculations of Model 3. For the 1S_0 ground state the resulting MR set was $\{1s^22s^2, 1s^22p^2, 1s^23p^2, 2s^23s^2, 2s^23p^2, 1s^23d^2\}$ and for the 1P_1 excited state the resulting MR set was $\{1s^22s2p, 1s^22p3d, 2s2p3s^2, 2s2p3p^2\}$. All the orbitals occupied in MR set were spectroscopically treated in the lowest order of approximation. Then the correlation orbitals were treated in the same way as those of Model 3 using the EOL scheme.

E. Models: summary

Our approach with either a common or two separate set of orbitals for the ground and excited states combines the strengths and weaknesses of the previous calculations which provide the uncertainty of the order of 10^{-3} [20, 23, 24]. The orbitals in the common set for both states are orthogonal to each other and there is no orbital overlap for the evaluation of the transition amplitude. At the same time, our procedure of two different sets of orbitals for each state has the advantage that the electron relaxation effects are automatically included to a large extent. In all our correlation models the overall conver-

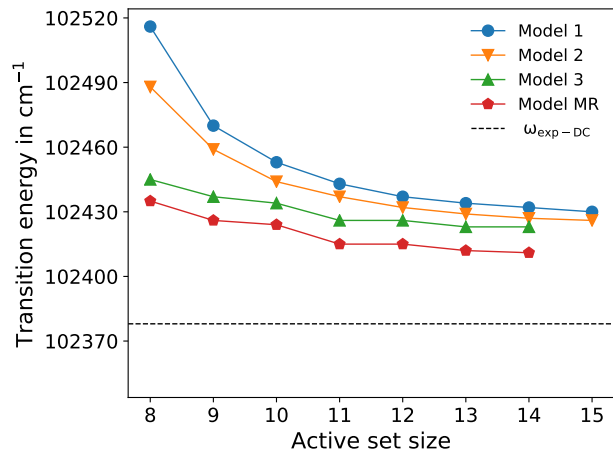


FIG. 4. Convergence of transition energy with respect to the increasing n of the active set size defining the wave function expansion for the VV+CV+CC:SDTQ calculations of different correlation models. Please see the text for the details of the VV+CV+CC:SDTQ calculations.

gence trends and behavior of the inner and outer electron correlations are consistent with each other. In Fig. 4 we present the convergence of the transition energy with respect to the increasing n of the active set size defining the wave function expansion for the VV+CV+CC:SDTQ calculations from all the correlation models under present study. For the Model 3 and MR we could not get the con-

verged orbitals for $n = 15$. The first three models vary just with a difference of maximum of 6 cm^{-1} . But for Model MR we get 15 cm^{-1} better results and this is obviously due to the inclusion of higher-order correlations in this model.

In Fig. 5 we present the line strength for the VV+CV+CC:SDTQ correlations calculated within Model 2, 3, and MR in a similar way as explained in Sec. III A and Fig. 2 (lower plot). From these plots, one can clearly see that in all models the line strength in the velocity adjusted to the experimental-Dirac-Coulomb energy agrees with the length gauge result much better than the adjusted to the pure experimental energy. This also confirms our expectations originated from the basic principles as stated at the end of Sec. III A. In order to get the final (Dirac-Coulomb) line strength value the results of the length gauge and adjusted to the experimental-Dirac-Coulomb energy velocity gauge obtained at the maximum active set size are analysed. The employed data from all the correlation models are summarized in Table II and Fig. 6. As one can see from these data, despite the extraordinary agreement between gauges, e.g., in Model 1, one can not use it for the uncertainty estimation. The reason for this has been explained at the end of Sec. II and confirmed now by the calculations in other models, which predict quite larger spread of the results than given by the difference of the gauges. We take an average of these scatter of the line strength data to predict the final value of the line strength and take one standard deviation of these scatter of the line strength data to predict the uncertainty in the results. As a result, present line strength accounting only the correlations is $2.43851(37)$. This is represented as a black solid line in Fig. 6, whereas in this figure the uncertainty is shown as a gray shaded region. We find rather conservative to assess the uncertainty as one standard deviation of the scattered data. Such kind of an error estimation is further supported by the fact that it covers all the values obtained in the length gauge, which is known to be more reliable.

TABLE II. ω is the Dirac-Coulomb transition energy (cm^{-1}). S^l and $S_{(\text{exp-DC})}^v$ are the Dirac-Coulomb line strengths in the length gauge and in the velocity gauge adjusted to $\omega_{\text{exp-DC}}$ energy (see text), in a.u.

Label	ω	S^l	$S_{(\text{exp-DC})}^v$
Model 1	102426	2.43843	2.43837
Model 2	102430	2.43820	2.43863
Model 3	102423	2.43869	2.43796
Model MR	102411	2.43854	2.43929
Final		2.43851(37)	

IV. NUCLEAR RECOIL CORRECTION

Once the line strength is calculated, including all the major correlation contributions, the finite nuclear mass

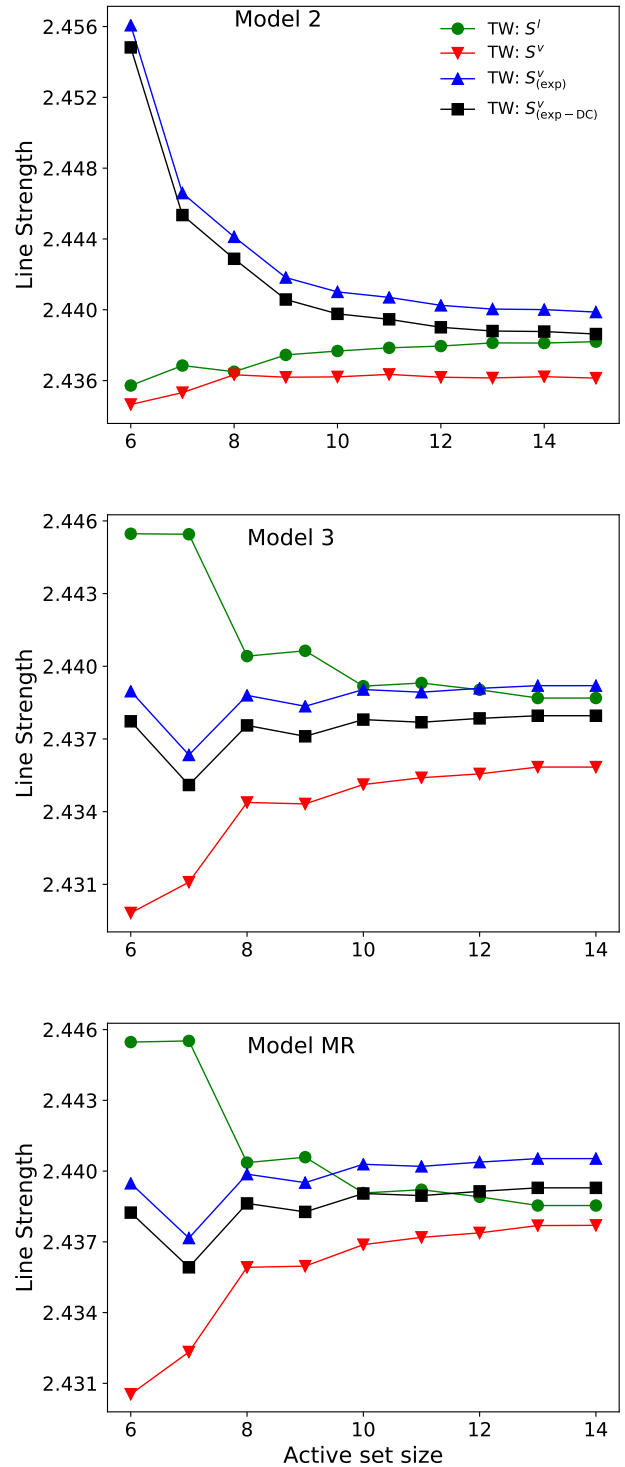


FIG. 5. Line strength for the for the VV+CV+CC:SDTQ calculations from the Model 2, Model 3 and Model MR plotted similarly as that of Fig. 2. In each sub-figure, the green circles are the line strength S^l in length form, red down triangles are *ab initio* S^v velocity from, blue upper triangles are $S_{(\text{exp})}^v$ velocity form adjusted the experimental transition energy ω_{exp} and black squares are $S_{(\text{exp-DC})}^v$ velocity from adjusted the experimental-Dirac-Coulomb transition energy $\omega_{\text{exp-DC}}$ (see text).

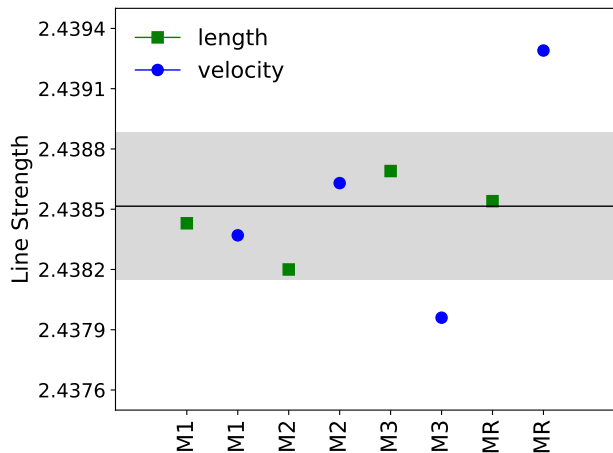


FIG. 6. Line strength of the $1s^2 2s 2p \ ^1P_1 - 1s^2 2s^2 \ ^1S_0$ transition in Be-like carbon plotted against the present Models. Green squares correspond to the length-form values and blue circles to the velocity-form values. The black solid line is the average of the both length and velocity forms. The gray shaded region is one standard deviation with respect to the black line.

(nuclear recoil) contribution was added as a correction given as

$$\Delta S_{\text{rec}} = \Delta S_{\text{rec,en}} + \Delta S_{\text{rec,wf}} + \Delta S_{\text{rec,op}}, \quad (10)$$

where the first two terms on the right side in Eq. (10) are the corrections to the line strength due to nuclear-recoil contributions to the energy and wave functions. These corrections were calculated using the relativistic configuration interaction (RCI) program of GRASP2K [25]. Here the lowest order nuclear motional corrections, namely the normal mass shift (NMS) term based on Dirac kinetic energy operator

$$\hat{H}_{\text{NMS}} = \frac{1}{M} \sum_{i=1}^N \left[c\alpha_i \cdot \mathbf{p}_i + (\beta_i - 1)c^2 \right],$$

where the M is the nuclear mass, and mass polarization term named as the specific mass shift (SMS)

$$\hat{H}_{\text{SMS}} = \frac{1}{M} \sum_{i < j=1}^N \mathbf{p}_i \cdot \mathbf{p}_j,$$

were added to the Dirac-Coulomb Hamiltonian, Eq. (1). The additional relativistic corrections to the recoil operators are of the order $(Z\alpha)^2$ [39]. For $Z = 6$, these corrections are in the order of 10^{-6} , which is far below than present level of uncertainty. However, the relativistic corrections must be taken into considerations for the future studies of higher Z .

It is also important, however, to take into account the recoil correction to the transition operator, i.e., the third term in Eq. (10). Previously, it was considered in

Refs. [37–40] for the $E1$ transitions and in Ref. [41] for the $M1$ -decay. Starting from the nonrelativistic Hamiltonian for N electrons and the nucleus, we obtain the following recoil corrections to the $E1$ transition operator:

$$\Delta \mathbf{T}_{\text{rec}}^l = -\frac{Z-N}{M} \sum_{i=1}^N \mathbf{r}_i \quad (11)$$

in the length gauge and

$$\Delta \mathbf{T}_{\text{rec}}^v = -\frac{Z}{M} \frac{1}{\omega} \sum_{i=1}^N \mathbf{p}_i \quad (12)$$

in the velocity gauge. From these expressions one can easily come to the corresponding corrections to the line strength

$$\begin{aligned} \Delta S_{\text{rec,op}}^l &= 2\text{Re} \left\{ \langle \Psi(\Gamma; \pi J) | | \mathbf{T}^l | | \Psi(\Gamma'; \pi' J') \rangle \right. \\ &\quad \times \left. \langle \Psi(\Gamma; \pi J) | | \Delta \mathbf{T}_{\text{rec}}^l | | \Psi(\Gamma'; \pi' J') \rangle \right\} \\ &\approx 2 \frac{Z-N}{M} S^l \end{aligned} \quad (13)$$

and

$$\begin{aligned} \Delta S_{\text{rec,op}}^v &= 2\text{Re} \left\{ \langle \Psi(\Gamma; \pi J) | | \mathbf{T}^v | | \Psi(\Gamma'; \pi' J') \rangle \right. \\ &\quad \times \left. \langle \Psi(\Gamma; \pi J) | | \Delta \mathbf{T}_{\text{rec}}^v | | \Psi(\Gamma'; \pi' J') \rangle \right\} \\ &\approx 2 \frac{Z}{M} S^v. \end{aligned} \quad (14)$$

In Table III different recoil contributions due to the en-

TABLE III. The recoil corrections to the line strength originated from the energy and wave functions change, $\Delta S_{\text{rec,en+wf}}$, as well as due to the transition operator $\Delta S_{\text{rec,op}}$ calculated in the length and velocity gauges. The total gauge invariant recoil correction is presented in the last line. The values are in a.u.

Rec. correction	length	velocity
$\Delta S_{\text{rec,en+wf}}$	0.00000	-0.00089
$\Delta S_{\text{rec,op}}$	0.00045	0.00134
Total	0.00045	0.00045

ergy, wave functions, and operator are presented in the length and velocity gauges. Only with the term due to the change of the operator included the total recoil correction is gauge invariant. In view of this, we would recommend to introduce this contribution also to the next GRASP update.

V. DISCUSSION AND CONCLUSION

With the discussion above, we can obtain the final value of the line strength. In order to do so, we add to the Dirac-Coulomb value 2.43851(37) from Sec. III the recoil correction $\Delta S_{\text{rec}} = 0.00045$ calculated in the

previous section. In addition, we have to consider also other effects, such as the Breit interaction as well as QED. The Breit contribution has been calculated as follows. The frequency-independent Breit Hamiltonian has been added to the Dirac-Coulomb Hamiltonian given by Eq. (1). Then the RCI calculations have been performed within the correlation Model 1. Comparing further the obtained results with the corresponding Dirac-Coulomb values we get for the Breit contribution ΔS_{Breit} 0.00030 and -0.00001 in the length and velocity gauge, respectively. Based on an analysis of the Breit contribution in the intercombination transition $2s2p\ ^3P_1 - 2s^2\ ^1S_0$ in Be-like carbon Ref. [23] and on arguments presented in Refs. [48, 49], we attribute this difference to the negative-energy corrections. That means that the gauge invariance of the Breit contribution should be restored when the negative-energy states will be accurately taken into account. On the other hand, it was demonstrated [48, 49], that the negative-continuum affects dominantly only the result in the velocity gauge, while the result of the length gauge remains stable. In view of this, we add the Breit correction calculated in the length gauge and with the 50% uncertainty, $\Delta S_{\text{Breit}} = 0.00030(15)$, to our final value. The remaining QED correction is estimated as $\alpha(\alpha Z)^2 \ln(\alpha Z)^{-1}$ [50, 51] to be 4×10^{-5} , which is much smaller than our uncertainty. As a result, our final value for the line strength reads 2.43926(40), where the uncertainty is coming from the correlations and Breit contribution.

Once the line strength is calculated, it is straightforward to get the weighted oscillator strength gf :

$$gf = \frac{2}{3}\omega S, \quad (15)$$

TABLE IV. Comparisons between different calculations and experiments for the line strength of the $1s^22s2p\ ^1P_1 - 1s^22s^2\ ^1S_0$ transition and the lifetime of the $1s^22s2p\ ^1P_1$ excited state in Be-like carbon.

S [a.u.]	τ [ns]	Ref.
Theories		
2.434(6)	0.5673(13)	[18]
2.435(6)	0.5671(13)	[19]
2.4376(13)	0.56650(30)	[20]
2.057	0.6713	[22]
2.4377(10)	0.56648(23)	[23]
2.4390(24)	0.56618(55)	[24]
2.436	0.5669	[21]
2.43926(40)	0.56612(9)	Present work
Experiments		
2.09(1)	0.66(3)	[42]
2.16(2)	0.64(6)	[43]
2.09(2)	0.66(7)	[44]
2.76(1)	0.50(3)	[45]
2.42(1)	0.57(2)	[46]
2.426(45)	0.569(10)	[47]

and the lifetime of the $1s^22s2p\ ^1P_1$ excited state:

$$\tau = \frac{3g}{4} \frac{c^3}{\omega^3 S}, \quad (16)$$

where g is the weight of the upper state. Here the conversion to the lifetime from the line strength and vice versa is performed by using the experimental energy, $\omega = 102352.04\ \text{cm}^{-1}$ [33]. We note that the present uncertainty in the lifetime is only due to calculated line strength, since the uncertainty of the transition energy is expected to be much better than $1\ \text{cm}^{-1}$ and this is far below the uncertainty of the line strength.

Fig. 7 and Table IV compare the present results of calculated line strength and lifetime with other theories and experiments. Note that in the respective papers the values of oscillator strength is provided. We have converted the oscillator strength to the line strength using the energies mentioned in the respective papers. In Fig. 7, the experimental line strength reported in Ref. [47] is plotted as a function of the experimental energy taken from the NIST database [33]. It is clear from Fig. 7 that our calculated energy is the closest to the experimental one. The present line strength or lifetime agrees very well with the CI+MBPT calculation of Savukov [24] and is in a fair agreement with the large-scale MCDF calculation of Jönsson and Froese Fischer [20] and the CI result of Chen, Cheng and Johnson [23].

It is obvious from the Table IV that all the theoretical lifetimes except of Ref. [22] are inside the error bar of the best available experimental lifetime of 0.569(10) ns [47]. However, the uncertainty of this measurement is still too large to distinguish between different theories. Therefore, we hope that the proposed experiment in Ref. [15] will provide a new benchmark for testing the theories in the case of Be-like carbon.

In conclusion, we have presented high precision atomic calculations of the line strength of the $1s^22s2p\ ^1P_1 -$

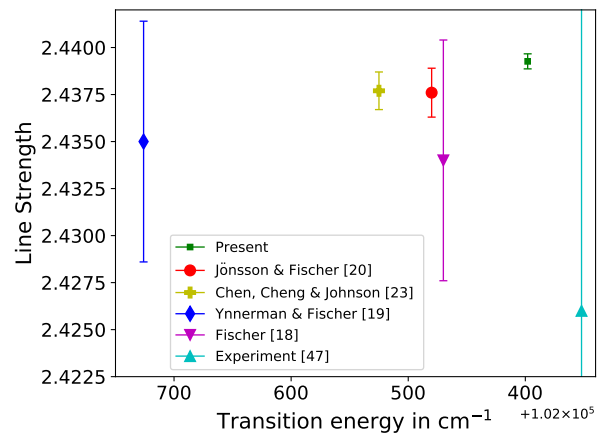


FIG. 7. A comparison of the present line strength of the $1s^22s2p\ ^1P_1 - 1s^22s^2\ ^1S_0$ transition in Be-like carbon with other theories and experiment.

$1s^2 2s^2 \ ^1S_0$ spin allowed $E1$ transition in Be-like carbon. We have utilized the state-of-the-art multiconfiguration Dirac-Hartree-Fock method. In these systematically enlarged wave functions, we incorporated higher-order electron correlations, where the orbital relaxation and overlaps are taken into account by using separate and simultaneous sets of relativistic orbitals in the active set. This helped us to reliably estimate the uncertainty of the obtained line strength. Moreover, the finite nuclear mass correction to the line strength is calculated by correcting the energy, wave functions as well as the transition

operator. The achieved relative uncertainty of the line strength amounts to 10^{-4} , which represents a reliable theoretical benchmark of the $E1$ line strength in a view of upcoming high precision lifetime measurement of the $1s^2 2s 2p \ ^1P_1$ state of Be-like carbon.

Extensions of current studies to heavier Be-like ions allow us to improve the theoretical accuracy of transition rates. The given (numerical) uncertainty together with the high precision experiments will allow an alternative spectroscopic test than the energy alone and will provide further insight into the atomic structure of many-electron atoms and ions.

-
- [1] X. Zhang and J. Ye, National Science Review **3**, 189 (2016).
- [2] J. R. C. López-Urrutia, Journal of Physics: Conference Series **723**, 012052 (2016).
- [3] S. Kraft-Bermuth, D. Hengstler, P. Egelhof, C. Enss, A. Fleischmann, M. Keller, and T. Stöhlker, Atoms **6**, 040059 (2018).
- [4] A. V. Volotka, D. A. Glazov, G. Plunien, and V. M. Shabaev, Annalen der Physik **525**, 636 (2013).
- [5] V. M. Shabaev, A. I. Bondarev, D. A. Glazov, M. Y. Kaygorodov, Y. S. Kozhedub, I. A. Maltsev, A. V. Malyshev, R. V. Popov, I. I. Tupitsyn, and N. A. Zubova, Hyperfine Interactions **239**, 60 (2018).
- [6] M. S. Safronova, D. Budker, D. DeMille, D. F. J. Kimball, A. Derevianko, and C. W. Clark, Rev. Mod. Phys. **90**, 025008 (2018).
- [7] E. Träbert, Atoms **2**, 15 (2014).
- [8] E. Träbert, Journal of Physics B: Atomic, Molecular and Optical Physics **43**, 074034 (2010).
- [9] A. Lapiere, U. D. Jentschura, J. R. Crespo López-Urrutia, J. Braun, G. Brenner, H. Bruhns, D. Fischer, A. J. González Martínez, Z. Harman, W. R. Johnson, C. H. Keitel, V. Mironov, C. J. Osborne, G. Sikler, R. Soria Orts, V. Shabaev, H. Tawara, I. I. Tupitsyn, J. Ullrich, and A. Volotka, Phys. Rev. Lett. **95**, 183001 (2005).
- [10] G. Brenner, J. R. C. López-Urrutia, Z. Harman, P. H. Mokler, and J. Ullrich, Phys. Rev. A **75**, 032504 (2007).
- [11] A. H. Zewail, The Journal of Physical Chemistry A **104**, 5660 (2000).
- [12] J. F. Sell, B. M. Patterson, T. Ehrenreich, G. Brooke, J. Scoville, and R. J. Knize, Phys. Rev. A **84**, 010501 (2011).
- [13] B. M. Patterson, J. F. Sell, T. Ehrenreich, M. A. Gearba, G. M. Brooke, J. Scoville, and R. J. Knize, Phys. Rev. A **91**, 012506 (2015).
- [14] E. Träbert, Applied Physics B **114**, 167 (2014).
- [15] J. Rothhardt, M. Bilal, R. Beerwerth, A. V. Volotka, V. Hilbert, T. Stöhlker, S. Fritzsche, and J. Limpert, X-Ray Spectrometry (In Press 2019).
- [16] S. Demmler, J. Rothhardt, S. Hädrich, M. Krebs, A. Hage, J. Limpert, and A. Tünnermann, Opt. Lett. **38**, 5051 (2013).
- [17] J. Rothhardt, S. Hädrich, S. Demmler, M. Krebs, S. Fritzsche, J. Limpert, and A. Tünnermann, Phys. Rev. Lett. **112**, 233002 (2014).
- [18] C. F. Fischer, Physica Scripta **49**, 323 (1994).
- [19] A. Ynnerman and C. F. Fischer, Phys. Rev. A **51**, 2020 (1995).
- [20] P. Jönsson and C. Froese Fischer, Phys. Rev. A **57**, 4967 (1998).
- [21] K. Wang, Z. B. Chen, C. Y. Zhang, R. Si, P. Jansson, H. Hartman, M. F. Gu, C. Y. Chen, and J. Yan, Astrophys. J. Suppl. Ser. **234**, 40 (2018).
- [22] U. I. Safronova, W. R. Johnson, M. S. Safronova, and A. Derevianko, Physica Scripta **59**, 286 (1999).
- [23] M. H. Chen, K. T. Cheng, and W. R. Johnson, Phys. Rev. A **64**, 042507 (2001).
- [24] I. M. Savukov, Phys. Rev. A **70**, 042502 (2004).
- [25] P. Jönsson, G. Gaigalas, J. Bieroń, C. F. Fischer, and I. Grant, Comput. Phys. Commun. **184**, 2197 (2013).
- [26] I. P. Grant, *Relativistic Quantum Theory of Atoms and Molecules: Theory and Computation* (Springer, New York, 2007).
- [27] C. F. Fischer, M. Godefroid, T. Brage, P. Jönsson, and G. Gaigalas, Journal of Physics B: Atomic, Molecular and Optical Physics **49**, 182004 (2016).
- [28] K. Dyall, I. Grant, C. Johnson, F. Parpia, and E. Plummer, Comput. Phys. Commun. **55**, 425 (1989).
- [29] I. M. Savukov and W. R. Johnson, Phys. Rev. A **62**, 052506 (2000).
- [30] P. Indelicato, V. M. Shabaev, and A. V. Volotka, Phys. Rev. A **69**, 062506 (2004).
- [31] C. F. Fischer, Physica Scripta **T134**, 014019 (2009).
- [32] C. F. Fischer, Journal of Physics B: Atomic, Molecular and Optical Physics **43**, 074020 (2010).
- [33] A. Kramida, Yu. Ralchenko, J. Reader, and NIST ASD Team, NIST Atomic Spectra Database (ver. 5.6.1), [Online]. Available: <https://physics.nist.gov/asd> [2019, February 18]. National Institute of Standards and Technology, Gaithersburg, MD. (2018).
- [34] J. Olsen, M. R. Godefroid, P. Jönsson, P. A. Malmqvist, and C. F. Fischer, Phys. Rev. E **52**, 4499 (1995).
- [35] J. Bieroń, L. Filippin, G. Gaigalas, M. Godefroid, P. Jönsson, and P. Pyykkö, Phys. Rev. A **97**, 062505 (2018).
- [36] L. Filippin, R. Beerwerth, J. Ekman, S. Fritzsche, M. Godefroid, and P. Jönsson, Phys. Rev. A **94**, 062508 (2016).
- [37] Z. Fried and A. D. Martin, Il Nuovo Cimento **29**, 574 (1963).
- [38] Z.-C. Yan and G. W. F. Drake, Phys. Rev. A **52**, R4316 (1995).

- [39] S. G. Karshenboim, Phys. Rev. A **56**, 4311 (1997).
- [40] Z.-C. Yan, M. Tambasco, and G. W. F. Drake, Phys. Rev. A **57**, 1652 (1998).
- [41] A. V. Volotka, D. A. Glazov, G. Plunien, V. M. Shabaev, and I. I. Tupitsyn, The European Physical Journal D **48**, 167 (2008).
- [42] L. Heroux, Phys. Rev. **180**, 1 (1969).
- [43] M. C. Poulizac and J. P. Buchet, Physica Scripta **4**, 191 (1971).
- [44] M. C. Buchet-Poulizac and J. P. Buchet, Physica Scripta **8**, 40 (1973).
- [45] M.-W. Chang, The Astrophysical Journal **211**, 300 (1977).
- [46] N. Reistad, R. Hutton, A. E. Nilsson, I. Martinson, and S. Mannervik, Physica Scripta **34**, 151 (1986).
- [47] N. Reistad and I. Martinson, Phys. Rev. A **34**, 2632 (1986).
- [48] W. Johnson, D. Plante, and J. Sapirstein (Academic Press, 1995) pp. 255 – 329.
- [49] A. Derevianko, I. M. Savukov, W. R. Johnson, and D. R. Plante, Phys. Rev. A **58**, 4453 (1998).
- [50] V. G. Ivanov and S. G. Karshenboim, Physics Letters A **210**, 313 (1996).
- [51] J. Sapirstein, K. Pachucki, and K. T. Cheng, Phys. Rev. A **69**, 022113 (2004).